THE UNCERTAINTIES IN THE ^{22}Ne+α-CAPTURE REACTION RATES AND THE PRODUCTION OF THE HEAVY MAGNESIUM ISOTOPES IN ASYMPTOTIC GIANT BRANCH STARS OF INTERMEDIATE MASS

A. I. KARAKAS[1,2,3]

Institute for Computational Astrophysics, Department of Astronomy and Physics, Saint Mary's University, Halifax,
NS B3H 3C3, Canada; akarakas@ap.smu.ca

M. A. LUGARO[4]

Institute of Astronomy, University of Cambridge, Madingley Road,
Cambridge CB3 0HA, UK; mal@ast.cam.ac.uk

AND

M. WIESCHER, J. GÖRRES, AND C. UGALDE[5]

Joint Institute for Nuclear Astrophysics, Department of Physics, University of Notre Dame, Notre Dame, IN 46556;
mwiesche@nd.edu, goerres.1@nd.edu, ugalde.1@nd.edu

ABSTRACT

We present new rates for the ^{22}Ne(α, n)^{25}Mg and ^{22}Ne(α, γ)^{26}Mg reactions, with uncertainties that have been considerably reduced compared to previous estimates, and we study how these new rates affect the production of the heavy magnesium isotopes in models of intermediate-mass asymptotic giant branch (AGB) stars of different initial compositions. All the models have deep third dredge-up, hot bottom burning, and mass loss. Calculations have been performed using the two most commonly used estimates of the ^{22}Ne+α rates as well as the new recommended rates, and with combinations of their upper and lower limits. The main result of the present study is that, with the new rates, uncertainties on the production of isotopes from Mg to P coming from the ^{22}Ne+α-capture rates have been considerably reduced. We have therefore removed one of the important sources of uncertainty to effect models of AGB stars. We have studied the effects of varying the mass-loss rate on nucleosynthesis and discuss other uncertainties related to the physics employed in the computation of stellar structure, such as the modeling of convection, the inclusion of a partial mixing zone, and the definition of convective borders. These uncertainties are found to be much larger than those coming from ^{22}Ne+α-capture rates, when using our new estimates. Much effort is needed to improve the situation for AGB models.

Subject headings: nuclear reactions, nucleosynthesis, abundances — stars: AGB and post-AGB — stars: evolution — stars: interiors

1. INTRODUCTION

The origin of the stable magnesium isotopes, ^{24}Mg, ^{25}Mg, and ^{26}Mg, is of particular interest to astrophysics because Mg is one of the few elements for which we can obtain isotopic information from stellar spectroscopy. The ratio ^{24}Mg:^{25}Mg:^{26}Mg has been derived from high-resolution spectra of cool dwarfs and giants in the thin and thick disk of the Galaxy (Gay & Lambert 2000; Yong et al. 2003b) and for giants stars in the globular cluster (GC) NGC 6752 (Yong et al. 2003a). These observations show that many of the stars, including relatively metal-poor stars ([Fe/H] $\lesssim$ −1.0), have nonsolar Mg isotopic ratios[6] with enhancements in the neutron-rich isotopes, ^{25}Mg and ^{26}Mg, compared to what is expected from galactic chemical evolution (GCE) models. The main stellar nucleosynthesis site for all three stable isotopes is hydrostatic burning in the carbon and neon shells of massive stars that explode as Type II supernovae (Woosley & Weaver 1995; Chieffi & Limongi 2004). The abundances of the neutron-rich Mg isotopes are further enhanced by secondary α-capture processes operating in the helium shell. The amount of ^{24}Mg produced does not strongly depend on the initial metallicity of the model and is an example of primary nucleosynthesis,[7] whereas the amounts of ^{25}Mg and ^{26}Mg produced scale with the initial metallicity of the star. This means that the Mg content of the ejecta of low-metallicity supernovae will be mostly ^{24}Mg with very little ^{25}Mg and ^{26}Mg produced, with typical ratios ^{24}Mg:^{25}Mg:^{26}Mg $\approx$ 99.0:0.50:0.50 from a 25 $M_{\odot}$ supernova model with metallicity $Z = 0.01\,Z_{\odot}$ (Woosley & Weaver 1995).

Previous studies have shown that GCE models using ejecta from massive stars match the observational data well for [Fe/H] > −1.0 but severely underestimate ^{25,26}Mg/^{24}Mg at lower metallicities (Timmes et al. 1995), indicating that another production

---

[1] Swinburne Centre for Astrophysics and Supercomputing, Swinburne University, Mail 31, P.O. Box 218, Hawthorn, VIC 3122, Australia.

[2] Centre for Stellar and Planetary Astrophysics, Monash University, Clayton, VIC 3800, Australia.

[3] Current address: Origins Institute, Department of Physics and Astronomy, McMaster University, Hamilton, ON L8S 4M1, Canada.

[4] Current address: Astronomical Institute, Utrecht University, Princetonplein 5, 3584 CC Utrecht, Netherlands.

[5] Current addresses: Department of Physics and Astronomy, University of North Carolina, CB 3255, Chapel Hill, NC 27599; and Triangle Universities Nuclear Laboratory, Duke University, CB 90308, Durham, NC 27708.

[6] The solar Mg isotopic ratios are ^{24}Mg:^{25}Mg:^{26}Mg = 79 : 10 : 11 (Lodders 2003).

[7] Primary production means that the species is produced from the hydrogen and helium initially present in the star, and the amount produced is relatively independent of the metallicity, Z, whereas secondary production requires some heavier seed nuclei to be present, and the amount produced scales with Z.

site for the neutron-rich Mg isotopes at low metallicities is required to account for the observations. Recently, Fenner et al. (2003) included the predicted stellar yields of ^{25}Mg and ^{26}Mg from AGB stars (Karakas & Lattanzio 2003) along with yields from Type II supernovae (Woosley & Weaver 1995; Chieffi & Limongi 2002) into a GCE model of the solar neighborhood. The GCE model with the AGB contribution could successfully match the Mg isotopic ratios of the metal-poor Galactic disk stars, while the model without an AGB contribution could not. This result indicates that low-metallicity intermediate-mass AGB stars may play an important role in the production of these species in galaxies and stellar systems. The production of the neutron-rich isotopes in AGB stars is also of interest in relation to the nonsolar Mg isotopic ratios observed in giant stars in GCs (Yong et al. 2003a, 2006). The nonsolar Mg isotopic ratios observed in NGC 6752 have been attributed to AGB stars, but Fenner et al. (2004) used a GCE model with tailor-made AGB yields from Campbell et al. (2005) and failed to match the abundance patterns observed in stars in that cluster. As Ventura & D'Antona (2005a, 2005b) have pointed out, there are still many uncertainties that effect the stellar yields, so an AGB solution to the GC anomalies cannot be ruled out at present.

Further motivation for the study of the production of the Mg isotopes in AGB stars is given by their relevance in the important current debate on the apparent variation of the fine-structure constant (Murphy et al. 2001; Ashenfelter et al. 2004; Fenner et al. 2005) and the origin of presolar spinel grains, some of which show enhancements in both ^{25}Mg and ^{26}Mg compared to solar (Zinner et al. 2005).

Briefly, intermediate-mass stars (initial mass ~ 4–8 $M_{\odot}$) will enter the thermally pulsing (TP) phase with a hydrogen (H) exhausted core mass (hereafter core mass) $M_c \gtrsim 0.8$ $M_{\odot}$, after experiencing the second dredge-up (SDU; Lattanzio et al. 1996; Busso et al. 1999; Herwig 2005). The SDU brings the products of H burning to the stellar surface (mostly ^{4}He and ^{14}N) and will slightly alter the composition of the Mg isotopic ratios, with an enrichment in ^{26}Mg at the expense of ^{25}Mg. For the massive $Z = 0.0001$ models, the SDU is the first time the surface abundances are altered, because there is essentially no first giant branch phase (Herwig 2004a). Following the SDU, the He-burning shell becomes thermally unstable and flashes every few thousand years or so. The energy from the thermal pulse (TP) drives a convective pocket in the He-rich intershell, which thoroughly mixes the products of He nucleosynthesis within this region. Following the TP, the convective envelope moves inward in mass and may reach the region previously mixed by the flash-driven convective pocket. This mixing event is known as the third dredge-up (TDU) and, if it occurs, is responsible for enriching the envelope in material from the H-exhausted core. Following the TDU the star contracts and the H shell is reignited and provides nearly all of the surface luminosity for the next interpulse period. The TP–TDU–interpulse cycle may occur many times during the TP-AGB phase; how many times depends on a number of factors, including the convective model, which determines the surface luminosity and mass-loss rate and hence the total AGB lifetime (Ventura & D'Antona 2005a).

Hot bottom burning (HBB) can also occur when the base of the convective envelope becomes hot enough to sustain proton capture nucleosynthesis (Lattanzio et al. 1996). If the temperature at the base of the envelope is sufficiently hot (over $\sim 60 \times 10^6$ K), the NeNa and MgAl chains may operate alongside the CNO cycle; ^{7}Li production is also possible via the Cameron-Fowler mechanism (Sackmann & Boothroyd 1992; Lattanzio et al. 1996), which operates at lower temperatures [typically $\sim (30$–$40) \times 10^6$ K]. Frost et al. (1998) noted that intermediate-mass AGB stars may
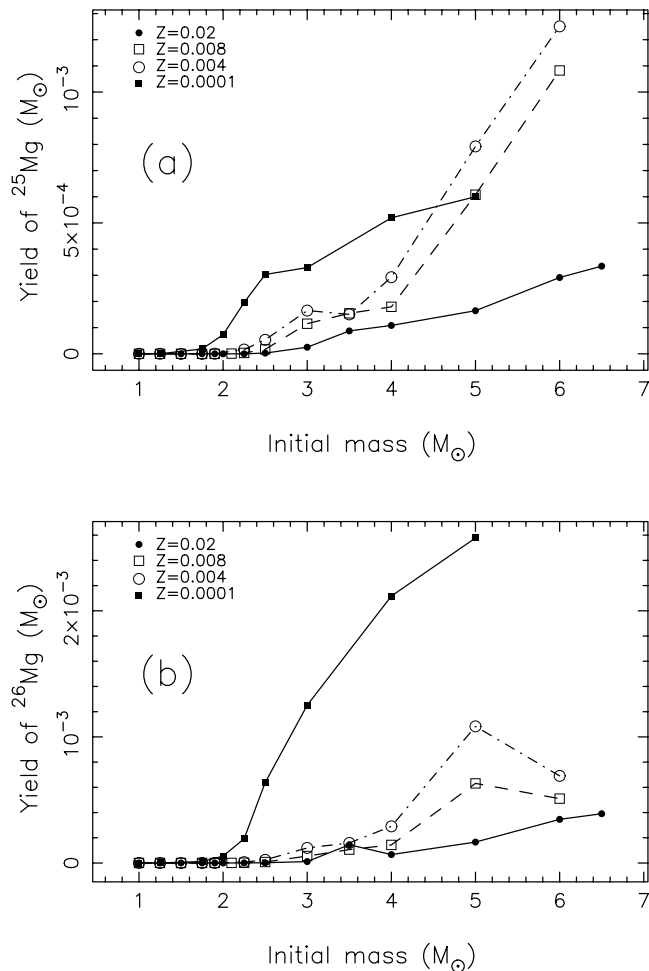

FIG. 1.—Stellar yields of (*a*) ^{25}Mg and (*b*) ^{26}Mg (in solar masses) as a function of mass and metallicity, from Karakas & Lattanzio (2003). Also included are the yields from the $Z = 0.0001$ AGB models. The reaction rates used for these models are our *standard* choice as outlined in the text. We define the stellar yield to be $y_k = \int_{\tau} [X(k) - X_0(k)](dM/dt)\,dt$, where τ is the stellar lifetime, $X(k)$ is the current mass fraction, $X_0(k)$ is the initial mass fraction, and dM/dt is current mass-loss rate.

become luminous, optically obscured carbon stars near the end of the TP-AGB, when mass loss has removed much of the envelope, extinguishing HBB but allowing dredge-up to continue.

Karakas & Lattanzio (2003) described in detail the various nucleosynthesis processes that alter the Mg isotopic ratios in AGB stars. To summarize, ^{25}Mg and ^{26}Mg are synthesized in the He shell during TPs by the reactions ^{22}Ne$(\alpha, n)^{25}$Mg and ^{22}Ne$(\alpha, \gamma)^{26}$Mg, when the temperature exceeds about 300×10^6 K. The amount of Mg produced depends on the thermodynamic conditions inside the pulse as well as on the composition of the intershell, which will have been altered by previous H and He burning. Neutron captures, in particular the ^{25}Mg$(n, \gamma)^{26}$Mg reaction, can also alter the Mg isotopic ratio in the intershell, where the neutrons come from the ^{22}Ne$(\alpha, n)^{25}$Mg reaction (Herwig 2004b). HBB can also significantly alter the surface Mg isotopic ratio via the activation of the MgAl chain, which can result in the destruction of ^{24}Mg if the temperature exceeds $\sim 90 \times 10^6$ K.

The stellar yields of ^{25}Mg and ^{26}Mg presented in Karakas & Lattanzio (2003) and shown in Figure 1 were calculated from models covering a range in mass (1–6 $M_{\odot}$) and metallicity ([Fe/H] = 0, -0.3, -0.7). From this figure we see that the most massive AGB models produce the most ^{25}Mg and ^{26}Mg, as a consequence of higher temperatures in the He shells compared to lower mass stars; we also note an increase in production at a given

mass with a decrease in metallicity. The computationally demanding nature of AGB models precluded a detailed study in that paper of the effect of the major uncertainties (mass loss, nuclear reaction rates, and convection). A recent comprehensive study by Ventura & D'Antona (2005a, 2005b) demonstrated that the predictive power of AGB models is still seriously undermined by these uncertainties. The theory of convection has a significant effect on the structure and nucleosynthesis (Ventura & D'Antona 2005a), while varying the mass-loss rate results in larger changes to the stellar yields than varying the nuclear reaction rates (Ventura & D'Antona 2005b). However, the magnitude of the errors associated with the relevant nuclear reaction rates is still one of the key questions concerning predictions of magnesium production in intermediate-mass AGB models. While the rates of the $^{14}N(\alpha,\gamma)^{18}F$ and $^{18}O(\alpha,\gamma)^{22}Ne$ reactions are well determined (Görres et al. 2000; Dababneh et al. 2003), the two key α-capture reaction rates, $^{22}Ne(\alpha,n)^{25}Mg$ and $^{22}Ne(\alpha,\gamma)^{26}Mg$, suffer from large uncertainties at the stellar energies appropriate for AGB stars (Koehler 2002). For example, at typical He-shell burning temperatures, $T \approx 300 \times 10^6$ K, the NACRE compilation (Angulo et al. 1999) gives an upper limit to the $^{22}Ne(\alpha,n)^{25}Mg$ reaction rate that is about 47 times larger than the recommended rate. At lower temperatures, the uncertainties are even larger.

The aims of this paper are twofold. First, we present new reaction rates for the two key α-capture reactions, with considerably reduced uncertainties compared to those given by the NACRE compilation. Second, we use these new rates within models of different metallicities ([Fe/H] $\approx$ 0, -0.3, -0.7, -2.3) for a typical mass (5 $M_\odot$) that produces the Mg isotopes during the TP-AGB phase. For each model we calculate the stellar yields and compare to previous nucleosynthesis calculations using older estimates of these reaction rates, including those by Herwig (2004b) and Ventura & D'Antona (2005a, 2005b). We also examine the effect of other model uncertainties, in particular the inclusion of a partial mixing zone and mass loss, on the stellar yields.

The paper is organized as follows. In § 2 we discuss the numerical method used for the stellar model calculations, including a discussion of the input physics used. In § 3 we present new rates for the $^{22}Ne+\alpha$-capture reactions. The results of the calculations are presented in § 4 and discussed in § 5.

2. THE NUMERICAL METHOD

We calculate the structure first and perform detailed nucleosynthesis calculations afterward, using a postprocessing algorithm. The stellar structure models were calculated with the Monash version of the Mount Stromlo Stellar Structure Program; see Frost & Lattanzio (1996) and references therein for details. Mass loss on the first giant branch is included using the Reimer's mass-loss prescription (Reimers 1975) with the parameter $\eta = 0.4$; on the AGB we use the formulation given by Vassiliadis & Wood (1993) in all models unless indicated otherwise. We calculate two models (5 $M_\odot$, $Z = 0.02$ and 0.0001) using Reimer's mass loss on the AGB with the parameter $\eta = 3.5$. Here we assume that the Vassiliadis & Wood (1993) and Reimers (1975) mass-loss prescriptions, derived for solar-like metallicities or those appropriate for the Magellanic Clouds, can be applied to $Z = 0.0001$ intermediate-mass AGB models without modification. The use of either mass-loss law results in a large number of TPs (up to $\sim$140).

All models were calculated from the zero-age main sequence to near the end of the TP-AGB phase. The occurrence of the TDU and HBB depend critically on the convection model used (Frost & Lattanzio 1996; Mowlavi 1999; Ventura & D'Antona 2005a) and the method for determining convective borders. Briefly, we use the standard mixing-length theory (MLT) for convective regions,

with a mixing-length parameter $\alpha = l/H_P = 1.75$, and determine the border by applying the Schwarzschild criterion. Hence, we do not include convective overshoot, in the usual sense. We do, however, search for a neutral border to the convective zone, in the manner described in detail by Lattanzio (1986), Frost & Lattanzio (1996), and Karakas et al. (2002). We note that this method has been shown to increase the efficiency of the TDU compared to models that strictly use the Schwarzschild criterion.

We performed detailed nucleosynthesis calculations using a postprocessing code that includes 74 species and time-dependent diffusive mixing in all convective zones (Cannon 1993). The details of the nucleosynthesis network are outlined in Lugaro et al. (2004), but we remind the reader that we include 59 light nuclei and 14 iron group species. We also add the fictional particle, g, to count the number of neutron captures occurring beyond ^{62}Ni (Lattanzio et al. 1996; Lugaro et al. 2004). Initial abundances are taken from Anders & Grevesse (1989) for the $Z = 0.02$ models, and we assume scaled solar for the $Z = 0.0001$ models. We assume an initially α-enhanced mixture typical of thin-disk stars (Reddy et al. 2003) for the 5 $M_\odot$, $Z = 0.008$, 0.004 models. The initial Mg isotopic ratios (e.g., $^{25}Mg/^{24}Mg$) are 21.9% and 35.2% less than solar in the $Z = 0.008$ and 0.004 models, respectively.

The bulk of the 506 reaction rates are from the REACLIB data tables (Thielemann et al. 1986), based on the 1991 updated version. Some of the proton, α, and neutron capture reaction rates have been updated according to the latest experimental results (see Lugaro et al. [2004] for details), and we calculate one set of models using these rates. We define this set to be our *standard* set, and the results from these computations are shown in Figure 1. In all the other sets of computed models, we have updated the proton capture rates for the NeNa and MgAl chains to those recommended by NACRE (see Table 7 in the Appendix for details of which proton capture rates have been updated). With this new set of updated rates, we study the effect of changing the $^{22}Ne+\alpha$ rates: we run models with our standard choice for these rates (Käppeler et al. [1994], without the inclusion of the 633 keV resonance; indicated as K94 in Table 6) with the NACRE recommended rates (indicated as NACRE in Table 6) and with our new recommended rates, as well as using combinations of the new upper and lower limits.

3. NUCLEAR STRUCTURE OF ^{26}Mg AND THE UNCERTAINTIES IN THE $^{22}Ne+\alpha$-REACTION RATES

The reaction rates for the $^{22}Ne+\alpha$-fusion processes are determined by the level structure of the compound nucleus ^{26}Mg above the α-threshold at $T_\alpha = 10.615$ MeV and near the neutron threshold $T_n = 11.093$ MeV. There is only very limited experimental and theoretical information available about possible natural parity resonances in that energy range, and both the $^{22}Ne(\alpha,\gamma)^{26}Mg$ as well as the $^{22}Ne(\alpha,n)^{25}Mg$ reaction rates have substantial uncertainties in the temperature range of stellar helium burning. These uncertainties have been a matter of debate for quite some time.

The uncertainty for the $^{22}Ne(\alpha,n)^{25}Mg$ reaction is mainly determined by the possible contribution of a low-energy 1^- resonance at 0.538 MeV, which has been observed both in photon-induced neutron emission (Berman et al. 1969) as well as in neutron capture measurements (Weigmann et al. 1976; Koehler 2002). Yet it is not clear how strongly this level is populated in the α-channel. Direct $^{22}Ne(\alpha,n)^{25}Mg$ measurements (Harms et al. 1991; Drotleff et al. 1993; Jaeger et al. 2001) were performed over the entire energy range down to the neutron threshold, but these measurements were handicapped by cosmic-ray–induced background in the neutron detectors; therefore, only an upper limit for the resonance strength was obtained. Also in a $^{22}Ne(^6Li, d)^{26}Mg$ α-transfer measurement (Giesen et al. 1994) only an upper limit for the

TABLE 1
LEVEL PARAMETERS FOR α UNBOUND STATES IN ^{26}Mg

E_x (MeV)	$E_\alpha^{\rm cm}$ (MeV)	J^π	$\Gamma_\gamma{}^{\rm a}$ (eV)	$\Gamma_n{}^{\rm a}$ (eV)	$\Gamma_\alpha{}^{\rm b}$ (eV)	$\Gamma_{\rm tot}{}^{\rm a}$ (eV)
10.693.........	0.078	4^+	$3^{\rm c}$	...	$1.7^{+18.3}_{-1.6} \times 10^{-46}$	3
10.945.........	0.33	$2^+, 3^-$	$3^{\rm c}$	...	$6.5^{+3.9}_{-6.2} \times 10^{-15}$	3
11.112.........	0.497	2^+	1.73	2577	$7.3^{+14.5}_{-6.3} \times 10^{-11}$	2580
11.153.........	0.538	1^-	4.79	14.4	$4.1^{+7.6}_{-3.8} \times 10^{-9}$	19.2
11.163.........	0.548	2^+	4.56	4640	$8.4^{+5.2}_{-3.5} \times 10^{-10}$	4650
11.171.........	0.556	2^+	$3^{\rm a,c}$	1.44	$1.2^{+0.6}_{-0.6} \times 10^{-9}$	20
11.183.........	0.568	1^-	$3^{\rm c}$	0.54	$7.6^{+2.6}_{-2.6} \times 10^{-9}$	3.54
11.194.........	0.579	2^+	$3^{\rm c}$	0	$3.1^{+1.6}_{-1.6} \times 10^{-9}$	3
11.274.........	0.659	2^+	3.24	540	$6.1^{+2.1}_{-2.1} \times 10^{-8}$	543
11.286.........	0.671	1^-	0.79	1256	$3.4^{+1.2}_{-1.2} \times 10^{-7}$	1257
11.310.........	0.695	1^-	$3^{\rm c}$	1.12	$5.8^{+1.5}_{-1.5} \times 10^{-6}$	4.1
11.326.........	0.711	1^-	$3^{\rm c}$	0.6	$9.4^{+3.2}_{-3.2} \times 10^{-6}$	3.6
11.328.........	0.713	1^-	3.6	424	$3.9^{+1.3}_{-1.3} \times 10^{-5}$	428

[a] Koehler (2002).
[b] Giesen et al. (1994).
[c] Estimated average value (Koehler 2002).

TABLE 2
RECOMMENDED RESONANCE STRENGTHS AS WELL AS THEIR UPPER AND LOWER LIMITS

E_x (MeV)	$E_\alpha^{\rm cm}$ (MeV)	J^π	$\omega\gamma_{(\alpha,\gamma)}$ (eV)	$\omega\gamma_{(\alpha,\gamma)}^{\rm ll}$ (eV)	$\omega\gamma_{(\alpha,\gamma)}^{\rm ul}$ (eV)
10.693..............	0.078	4^+	1.6×10^{-45}	1.2×10^{-46}	3.6×10^{-44}
10.945..............	0.330	$2^+, 3^-$	2.8×10^{-15}	1.8×10^{-15}	1.0×10^{-13}
11.112..............	0.497	2^+	2.4×10^{-13}	3.4×10^{-14}	7.3×10^{-13}
11.153..............	0.538	1^-	3.0×10^{-9}	2.1×10^{-10}	8.7×10^{-9}
11.163..............	0.548	2^+	4.1×10^{-12}	2.4×10^{-12}	6.7×10^{-12}
11.171..............	0.556	2^+	8.9×10^{-10}	4.5×10^{-10}	1.3×10^{-9}
11.183..............	0.568	1^-	1.9×10^{-8}	1.3×10^{-8}	2.4×10^{-8}
11.194..............	0.579	2^+	1.6×10^{-8}	7.5×10^{-9}	2.4×10^{-8}
11.274..............	0.659	2^+	1.8×10^{-9}	1.2×10^{-9}	2.5×10^{-9}
11.286..............	0.671	1^-	6.4×10^{-10}	4.2×10^{-10}	8.7×10^{-10}
11.310..............	0.695	1^-	3.6×10^{-5}	3.2×10^{-5}	4.0×10^{-5}
11.326..............	0.711	1^-	2.3×10^{-5}	1.6×10^{-5}	3.2×10^{-5}
11.328..............	0.713	1^-	9.9×10^{-7}	6.8×10^{-7}	1.3×10^{-6}

NOTE.—Recommended resonance strengths as well as their upper and lower limits for the ^{22}Ne$(\alpha, \gamma)^{26}$Mg reaction derived from the parameters listed in Table 1.

α spectroscopic factor $S_\alpha \leq 0.2$ was determined. The NACRE compilation (Angulo et al. 1999) has based the upper limit for the reaction rate on the direct ^{22}Ne(α, n) measurement by Drotleff et al. (1993). For the lower limit any contribution of this resonance was neglected. While more recent ^{22}Ne(α, n) studies have reduced the upper limit substantially (Jaeger et al. 2001), the proposed value is still substantially higher than suggested by the α-transfer data. A recent systematic reanalysis by Koehler (2002) of the ^{25}Mg(n, γ) measurement by Weigmann et al. (1976) pointed out on the basis of a careful **R**-matrix analysis of ^{25}Mg$(n, \gamma)^{26}$Mg data that at least three or more additional natural parity states could be expected above the neutron threshold. It was shown by Koehler (2002) that, in particular, the possible contribution of the 2^+ level at 11.112 MeV to the reaction rate does raise its uncertainty by more than an order of magnitude. In view of this debate, and in the absence of new data, it seems worthwhile to review the present status and suggest more reliable limits for the rate taking into account all of the currently available experimental information. There are discrepancies of about 9 keV between the excitation energies resulting from the α-capture measurements and the neutron capture studies. Since in this paper we concentrate on the contribution of the levels not observed in the α channel we adopt for consistency the excitation energies given by Koehler (2002). This has only an negligible impact on the overall rate, well below the quoted uncertainties.

3.1. The Reaction Rate of ^{22}Ne$(\alpha, n)^{25}$Mg

As outlined by Koehler (2002), several natural parity resonances near the neutron threshold can contribute significantly to the ^{22}Ne$(\alpha, n)^{25}$Mg reaction rate increasing the neutron production at low energies. The upper limits given by Koehler (2002) were scaled to the experimental upper limits of the resonance state at $E_\alpha^{\rm cm} = 0.538$ MeV ($E_x = 11.153$ MeV, $J^\pi = 1^-$) by Jaeger et al. (2001). As pointed out above, α-transfer measurements suggest a substantially lower α-strength for the $E_x = 11.153$ MeV level. While the experimental lower limit indicates a resonance strength of $\omega\gamma \leq 60$ neV, the transfer data reduce the upper limit considerably to $\omega\gamma \leq 27$ neV (see also Käppeler et al. 1994) after renormalization of the reference resonance.

Based on the data by Giesen et al. (1994) and Koehler (2002) we have reanalyzed the strength of the low-energy resonances and derived the resonance strength from the α spectroscopic factors

normalized to the newly determined strength of the well-known resonance at $E_\alpha^{\rm cm} = 0.713$ MeV ($E_x = 11.328$ MeV, $J^\pi = 1^-$; Jaeger et al. 2001). The procedure has been outlined in Giesen et al. (1994). Table 1 summarizes the level parameters adopted for determining the strengths as well as the upper and lower limits for the neutron unbound states between 11.1 and 11.4 MeV in ^{26}Mg. While neutron capture data (Weigmann et al. 1976; Koehler 2002) indicate a large number of natural parity states between 11.16 and 11.3 MeV excitation energy, no appreciable α-strength has been observed for these levels in the ^{22}Ne$(^6$Li, $d)^{26}$Mg transfer reaction. For these state levels we adopt an average spectroscopic strength of $C^2S_\alpha = 0.005$. For the two levels at 11.113 and 11.153 MeV at the neutron threshold the experimental data indicate some α-strength, which, however, could not be reliably determined due to the lack of experimental resolution in the deuteron spectrum. We extracted S_α spectroscopic factors of 0.005 and 0.01, respectively, with an upper limit of 0.01 and 0.02. For the neutron and γ-partial widths we adopted the values given by Koehler (2002) for calculating the resonance strengths. Using these resonance strengths listed in Table 3 we have calculated the reaction rate contributions of the resonances for ^{22}Ne$(\alpha, n)^{25}$Mg.

The reaction rate is shown as a function of temperature in Figure 2. In the temperature range between 0.3 and 0.5 GK the reaction rate is dominated by the contribution of the lowest measured resonance at $E_\alpha^{\rm cm} = 0.713$ MeV (Jaeger et al. 2001). At higher temperatures the rate is determined by higher energy resonance contribution resonances (Harms et al. 1991; Drotleff et al. 1993). The threshold resonance states determine the rate at lower temperatures ≤ 0.3 GK. The largest uncertainty is obviously associated with this low-temperature range. Based on the currently available data the reaction rate is uncertain by roughly 1 order of magnitude. This uncertainty depends mainly on the uncertainty in the spectroscopic α-strengths of the threshold resonances. More detailed experimental work is necessary to reduce the present uncertainties.

3.2. The Reaction Rate of ^{22}Ne$(\alpha, \gamma)^{26}$Mg

It has been argued before (Käppeler et al. 1994) that the ^{22}Ne$(\alpha, \gamma)^{26}$Mg reaction may compete strongly at low temperature with the ^{22}Ne$(\alpha, n)^{25}$Mg-capture process. This possibility depends sensitively on the contribution of resonances at energies

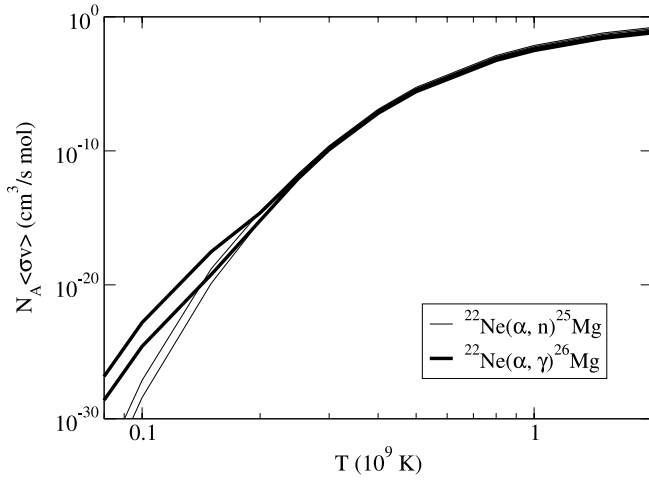FIG. 2.—Reaction rates for ^{22}Ne$(\alpha, n)^{25}$Mg and ^{22}Ne$(\alpha, \gamma)^{26}$Mg as a function of temperature. The solid lines represent the uncertainty range in the reaction rate as discussed in the text.

FIG. 3.—Ratio of the upper (lower) limits of the ^{22}Ne$(\alpha, n)^{25}$Mg and ^{22}Ne$(\alpha, \gamma)^{26}$Mg reaction rates and the recommended values as a function of temperature.

below the neutron threshold. Koehler (2002) has argued that the strong resonance at $E_\alpha^{cm} = 0.711$ MeV ($E_x = 11.326$ MeV, $J^\pi = 1^-$), which was observed by Wolke et al. (1989), does not correspond to the resonance level observed in the competing ^{22}Ne(α, n) reaction channel (Harms et al. 1991; Drotleff et al. 1993; Giesen et al. 1994; Jaeger et al. 2001). Only resonance levels with small neutron widths $\Gamma_n \leq \Gamma_\gamma$ can have an appreciable resonance strength in the ^{22}Ne(α, γ) channel.

We have recalculated the resonance strengths $\omega\gamma$ of all possible resonances in the ^{22}Ne(α, γ) channel. The resonance strengths scale directly with the spectroscopic factors S_α (Giesen et al. 1994), which have been renormalized to the experimentally determined strength of the state at 11.328 MeV (Jaeger et al. 2001). The spin parity assignment for the low-energy subneutron threshold resonances is based on the distorted-wave Born approximation analysis of the ^{22}Ne$(^6$Li, $d)^{26}$Mg data. The most important resonance is the one at $E_\alpha^{cm} = 0.33$ MeV ($E_x = 10.945$ MeV, $J^\pi = 2^+, 3^-$). The data do not allow a unique spin assignment for this level; this uncertainty represents the main uncertainty in the spectroscopic factor and resonance strength. These parameters were used to estimate the resonance strengths for the not yet observed low-energy resonances; the results are listed in Table 2.

TABLE 3
RECOMMENDED RESONANCE STRENGTHS AS WELL
AS THEIR UPPER AND LOWER LIMITS

E_x (MeV)	E_α^{cm} (MeV)	J^π	$\omega\gamma_{(\alpha, n)}$ (eV)	$\omega\gamma_{(\alpha, n)}^{ll}$ (eV)	$\omega\gamma_{(\alpha, n)}^{ul}$ (eV)
11.112..........	0.497	2^+	3.6×10^{-10}	5.0×10^{-11}	1.1×10^{-9}
11.153..........	0.538	1^-	9.2×10^{-9}	6.3×10^{-10}	2.6×10^{-8}
11.163..........	0.548	2^+	4.2×10^{-9}	2.4×10^{-9}	6.8×10^{-9}
11.171..........	0.556	2^+	4.3×10^{-10}	2.2×10^{-10}	6.5×10^{-10}
11.183..........	0.568	1^-	3.5×10^{-9}	2.3×10^{-9}	4.6×10^{-9}
11.274..........	0.659	2^+	3.0×10^{-7}	1.0×10^{-7}	4.1×10^{-7}
11.286..........	0.671	1^-	1.0×10^{-6}	6.6×10^{-7}	1.4×10^{-6}
11.310..........	0.695	1^-	4.7×10^{-6}	3.5×10^{-6}	6.0×10^{-6}
11.326..........	0.711	1^-	4.7×10^{-6}	3.1×10^{-6}	6.5×10^{-6}
11.328..........	0.713	1^-	1.18×10^{-4}	1.03×10^{-4}	1.33×10^{-4}

NOTE.—Recommended resonance strengths as well as their upper and lower limits for the ^{22}Ne$(\alpha, n)^{25}$Mg reaction derived from the parameters listed in Table 1.
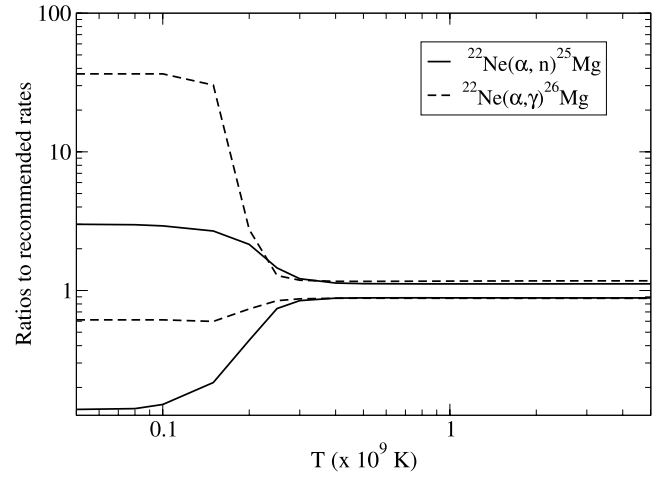
The reaction rate for ^{22}Ne$(\alpha, \gamma)^{26}$Mg is shown in Figure 2 as a function of temperature. For temperatures below 0.3 GK the resonance at $E_\alpha^{cm} = 0.33$ MeV clearly dominates the reaction rate; possible contributions can also come from the two 1^- resonances at $E_\alpha^{cm} = 0.538$ MeV ($E_x = 11.153$ MeV) and $E_\alpha^{cm} = 0.568$ MeV ($E_x = 11.183$ MeV) at the neutron threshold. Based on the recent reanalysis of the neutron capture data (Koehler 2002) these states are expected to have only small neutron partial widths. The reaction rate in the temperature range $T \geq 0.3$ GK is determined by the contributions of states above 11.3 MeV, in particular by the strong level at $E_\alpha^{cm} = 0.711$ MeV ($E_x = 11.326$ MeV), which has been measured by Wolke et al. (1989). Also indicated is the uncertainty range for the ^{22}Ne$(\alpha, \gamma)^{26}$Mg rate. It is obvious from this plot that the experimental uncertainties associated with the low-energy resonances dominate the uncertainty in the low-temperature range.

3.3. The Comparison of the Reaction Channels

The temperature dependence of the two ^{22}Ne$+\alpha$ reaction rates differ considerably at lower temperatures because the neutron channel opens only at higher energies. Figure 2 demonstrates that at low temperature $T \leq 0.2$ GK the (α, γ) reaction channel dominates over the competing (α, n) reaction process. However, there are still considerable uncertainties associated with the low-temperature range of the reaction rates as demonstrated in Figure 3. Shown are the upper and lower limits of the reaction rate normalized to the recommended value and clearly demonstrates that, below $T \leq 0.3$ GK, the uncertainty range rapidly increases toward lower temperatures to 1 order of magnitude for the ^{22}Ne$(\alpha, n)^{25}$Mg rate and to nearly 2 orders of magnitude for the ^{22}Ne$(\alpha, \gamma)^{26}$Mg rate. This affects the reliability for nucleosynthesis predictions in rapidly changing low-temperature environments. Figure 4 shows the ratios of ^{22}Ne$(\alpha, n)^{25}$Mg rate and ^{22}Ne$(\alpha, \gamma)^{26}$Mg rate. A comparison between the upper and lower limits of the respective reaction rates shows the uncertainty range for this ratio. At higher temperatures the ^{22}Ne$(\alpha, n)^{25}$Mg reaction clearly dominates, while toward lower temperatures the ^{22}Ne$(\alpha, \gamma)^{26}$Mg reaction will be far stronger than the competing ^{22}Ne$(\alpha, n)^{25}$Mg channel. However, the present data are not stringent enough to determine the exact temperature for this crossover but can be limited to a temperature range between 0.15 and 0.3 GK. Further measurements of low-temperature resonances in
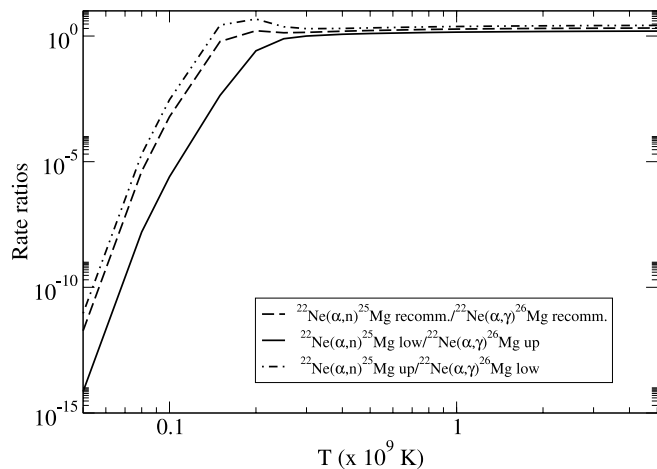
Fig. 4.—Ratio of the reaction rates of ^{22}Ne$(\alpha, n)^{25}$Mg and ^{22}Ne$(\alpha, \gamma)^{26}$Mg as a function of temperature. Shown are the ratio between the recommended values and the ratio between the upper limit of ^{22}Ne$(\alpha, n)^{25}$Mg and the lower limit of ^{22}Ne$(\alpha, \gamma)^{26}$Mg as upper limit for the overall uncertainty ratio as well as the ratio between the lower limit of ^{22}Ne$(\alpha, n)^{25}$Mg and the upper limit of ^{22}Ne$(\alpha, \gamma)^{26}$Mg as a lower limit for the ratio.

both reaction channels are therefore necessary to improve on the present uncertainties.

4. RESULTS

We now present the results of the stellar models. Unless otherwise stated, we discuss the models computed using the Vassiliadis & Wood (1993) mass-loss rates.

4.1. Structural Properties and the CNO Nuclei

In this section we present some of the structural properties of the stellar models used for the present study in detail, including a brief discussion of the evolution of the CNO nuclei during the TP-AGB phase. In Table 4 we first include the initial mass and metallicity and the mass-loss law adopted for the structure calculation. VW93 refers to models calculated with Vassiliadis & Wood (1993) mass loss, while R75 refers to models calculated with Reimers (1975) with the parameter $\eta_R = 3.5$. Futhermore, we present the core mass at the beginning of the TP-AGB, the mass of the envelope when HBB is shut off and the mass at the end of the calculation, the total number of TPs, the number of TDU episodes, the total amount of matter dredged into the envelope $M_{\mathrm{dred}}^{\mathrm{tot}}$, the maximum temperature at the base of the convective envelope, the maximum temperature in the He shell during a TP, and the maximum dredge-up efficiency, λ_{max}. In Table 5 we present some sur-

face abundances results including the final C+N+O value divided by the initial (see table caption for more details). The dredge-up efficiency is defined by $\lambda = \Delta M_{\mathrm{dredge}}/\Delta M_h$, where $\Delta M_{\mathrm{dredge}}$ is the amount of H-exhausted core matter mixed into the envelope and ΔM_h is the amount by which the core mass grew during the previous interpulse period. For all the models considered here, $\lambda \gtrsim 0.9$, is reached after a small number ($\sim$6) of pulses, similar to behavior observed by Stancliffe et al. (2004) and Herwig (2004a) for the same mass.

The VW93 mass-loss rate depends on the pulsation period until the period reaches 500 days, after which the luminosity-driven superwind phase begins. The pulsation period (Vassiliadis & Wood 1993) depends in turn on the radius and total mass, and because the lower metallicity models are more compact they take longer (in time) to reach the start of the superwind phase and hence experience more TPs than the solar metallicity models. In comparison, the R75 mass-loss rate is proportional to both the radius and the luminosity; and as we can see from Table 4 at the lowest metallicity we consider ($Z = 10^{-4}$) the large luminosity at this composition results in fewer TPs than using VW93 mass loss, the reverse of the behavior observed at $Z = 0.02$.

For all models except the $Z = 0.02$ cases, the temperature at the base of the envelope, T_{BCE}, increases quickly at the beginning of the TP-AGB and exceeds 50×10^6 K by about the eighth pulse. The envelope mass after which HBB is shut off decreases with a decrease in metallicity; see column (5) in Table 4. For the solar composition VW93 (R75) models, T_{BCE} reaches 50×10^6 K after about the 9th TP (12th TP) and decreases quickly once the envelope mass drops below $\approx$2.6 $M_\odot$, which is when HBB is shut off. After this, dredge-up continues increasing the C/O ratio above unity in some cases (see Table 5).

For the remainder of this section we summarize the nucleosynthesis of the CNO nuclei, because these species are not affected by varying the ^{22}Ne+α reaction rates. The contribution of many TPs with efficient dredge-up means that there is a considerable increase in the amount of ^{12}C that can be converted to primary ^{14}N by HBB (note also the low final ^{12}C/^{13}C ratios shown in Table 5). This increase can be best appreciated by comparing the final envelope C+N+O abundance (divided by the initial) for each model in Table 5. In the lowest Z models ^{14}N is the most abundant isotope, and an increase in Z results in decreasing levels of enrichment, where the final [^{14}N/Fe][8] values are 3.9, 1.9, 1.5, and 0.6 in the $Z = 0.0001$, 0.004, 0.008, and 0.02 models, respectively; [C/N] ratios have been observed in metal-poor stars in the halo, with the finding that $-0.5 < $ [C/N] < 1.5 at carbon

---

[8] Assuming solar values from Anders & Grevesse (1989), as used in the $Z = 0.02$ models. We use the standard logarithmic notation $[X/Y] = \log_{10}(X/Y)_* - \log_{10}(X/Y)_\odot$.

TABLE 4
Structural Properties of the 5 $M_\odot$ AGB Models

Z (1)	$\dot{M}$ (2)	$M_c(1)$ ($M_\odot$) (3)	$M_{\mathrm{env}}^{\mathrm{HBB}}$ ($M_\odot$) (4)	M_{env}^f ($M_\odot$) (5)	Number TP (6)	Number TDU (7)	$M_{\mathrm{dred}}^{\mathrm{tot}}$ ($M_\odot$) (8)	$T_{\mathrm{BCE}}^{\mathrm{max}}$ (10^6 K) (9)	$T_{\mathrm{He}}^{\mathrm{max}}$ (10^6 K) (10)	λ_{max} (11)
0.02	VW93	0.861	2.564	1.499	24	22	5.027($-$2)	64	352	0.961
0.02	R75	0.861	2.560	1.802	38	35	1.047($-$1)	57	368	0.977
0.008	VW93	0.870	1.857	1.387	59	56	1.745($-$1)	81	366	0.952
0.004	VW93	0.888	1.560	0.944	83	80	2.250($-$1)	85	379	0.959
10^{-4}	VW93	0.910	1.056	0.572	137	134	3.133($-$1)	92	380	0.980
10^{-4}	R75	0.909	1.100	0.335	70	67	1.569($-$1)	90	383	0.950

Note.—Structural properties of the 5 $M_\odot$ AGB models; see the text for details.

TABLE 5
Some Surface Abundance Results for the 5 $M_\odot$ Models

Z	$\dot{M}$	CNO_f/CNO_0	$^{12}C/^{13}C_f$	C/O_{agb}	C/O_f	Mg Ratio$_{agb}$	Mg Ratio$_f$
0.02.........................	VW93	1.341	7.828	0.291	0.766	$79.0:09.6:11.4$	$72.2:12.4:15.4$
0.02.........................	R75	1.814	15.57	0.291	1.705	$79.0:09.6:11.4$	$56.1:18.0:25.9$
0.008.......................	VW93	2.886	7.383	0.239	0.660	$82.8:07.6:09.6$	$46.1:19.6:34.2$
0.004.......................	VW93	5.106	10.77	0.204	2.102	$85.3:06.4:8.33$	$31.7:21.6:46.7$
10^{-4}.......................	VW93	431.1	9.223	0.209	9.400	$82.2:08.2:09.6$	$11.7:17.5:70.7$
10^{-4}.......................	R75	339.4	12.15	0.205	18.60	$82.2:08.2:09.6$	$04.5:16.7:78.7$

Note.—Some surface abundance results for the 5 $M_\odot$ models including the final C+N+O and $^{12}C/^{13}C$ ratio, and C/O ratio and the Mg isotope ratio ($^{24}Mg:^{25}Mg:^{26}Mg$) at the beginning and end of the TP-AGB phase (using the new recommended rates).

abundances around [C/Fe] ~ 2 (Johnson et al. 2005). Our models overproduce N compared to C, with [C/N] < -1 in all metal-poor 5 $M_\odot$ computations.

The solar-metallicity VW93 model does not become carbon-rich, whereas the R75 model becomes a carbon star after the 28th TP. From Table 4 we see that the reason for this is more TDU episodes, resulting in about a factor of 2 more matter dredged into the envelope. The 5 $M_\odot$, $Z = 0.008$ model does not become a carbon star, whereas the $Z = 0.004$ model does. The final [$^{12}C/Fe$] values for both cases are 0.16 and 0.70, compared to 0.09 and 0.16 initially. The $Z = 0.004$ model has a longer TP-AGB phase (0.59 Myr compared to 0.50 Myr), leading to more ^{16}O destroyed by HBB,

even though HBB temperatures are similar in both models. The final [$^{16}O/Fe$] values are 0.02 and 0.04, compared to the initial enhanced values of 0.16 and 0.24, respectively. The 5 $M_\odot$, $Z = 0.0001$ models (with VW93 and R75 mass loss) become carbon stars quickly, after the second TP. This is a consequence of deep TDU and a low initial ^{16}O envelope abundance. The final [$^{12}C/Fe$] values are 2.4 and 2.6 in the VW93 and R75 models. The envelope ^{16}O abundance is destroyed during the interpulse by HBB at temperatures $\approx 90 \times 10^6$ K, whereas the many efficient TDUs result in an overall increase, leading to a final [$^{16}O/Fe$] ≈ 1 in both cases. This behavior was also observed by Herwig (2004a) for the equivalent mass and metallicity.
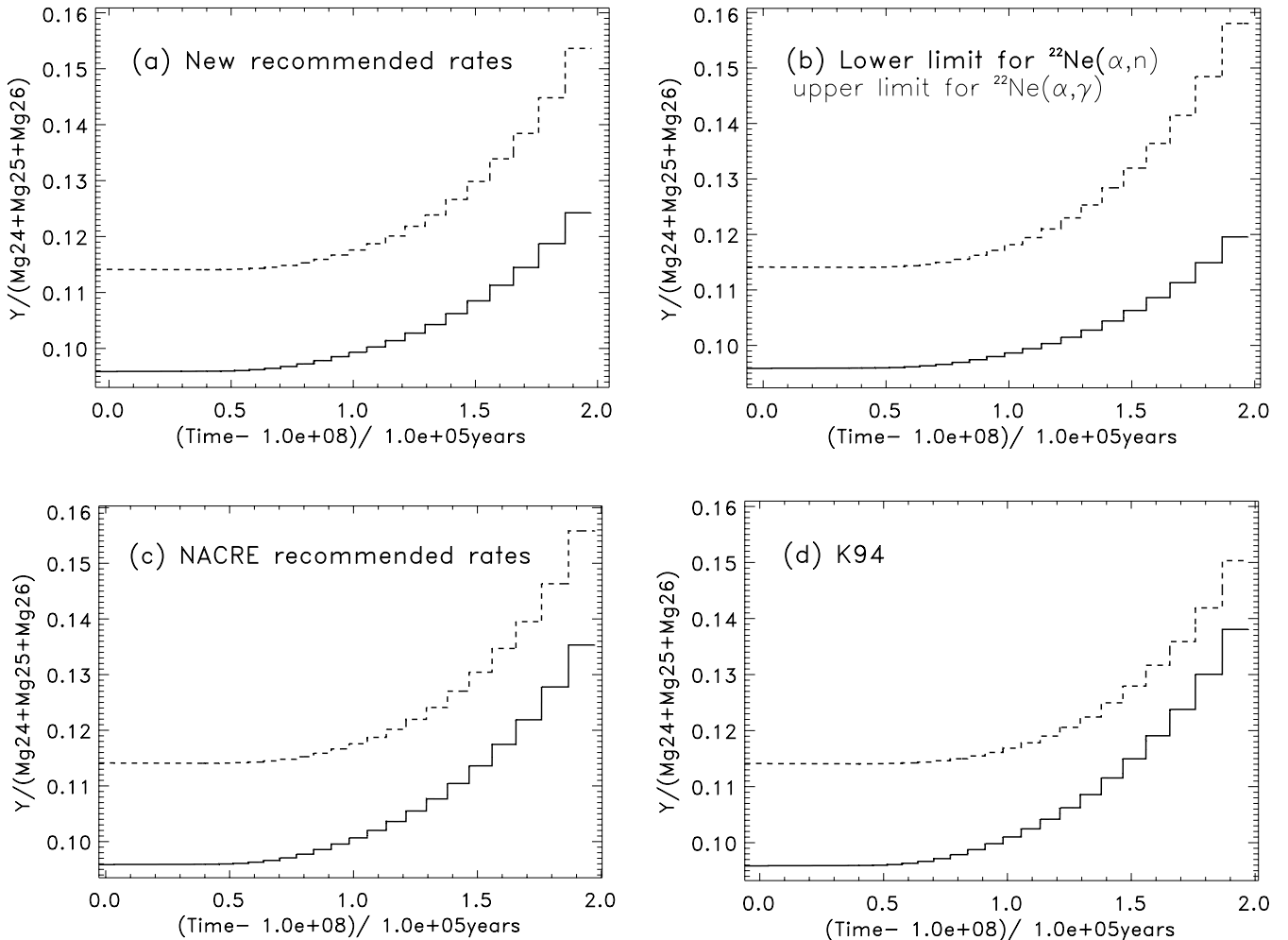

Fig. 5.—Evolution of the ^{25}Mg (solid lines) and ^{26}Mg (dashed lines) abundances at the surface of the 5 $M_\odot$, $Z = 0.02$ VW93 model for four different choices of the $^{22}Ne+\alpha$ reaction rates.

4.2. Surface Abundance Evolution of the Mg Isotopes

The envelope abundances of the Mg isotopes are first modified by the operation of the SDU, and the magnitude of such modifications increases with a decrease in the metallicity or an increase in the mass. For the 5 $M_\odot$, $Z = 0.02$, the envelope ^{25}Mg abundance decreases by 4.2% while ^{26}Mg increases by 3.7% after the SDU, whereas in the 5 $M_\odot$, $Z = 0.004$ model we observe a decrease of 9.4% in the ^{25}Mg abundance and an 8.4% increase in ^{26}Mg. For all cases but the 5 $M_\odot$, $Z = 0.0001$ model, the ^{24}Mg abundance does not change. For this model, the ^{24}Mg abundance increases by 11%, whereas the ^{25}Mg and ^{26}Mg abundances decrease by 13% and 6.8%, respectively. The results quoted above are for the calculations that use the NACRE NeNa and MgAl chain reaction rates.

In Figure 5 we show the evolution during the TP-AGB phase of the ^{25}Mg (*solid line*) and ^{26}Mg (*dashed line*) abundances at the surface of the 5 $M_\odot$, $Z = 0.02$ model for four different choices of the ^{22}Ne+α reaction rates. The abundances in Figure 5 are the mole fraction, Y (where the mass fraction $X = YA$ and A is the atomic mass), scaled to the total magnesium abundance, Mg $=$ ^{24}Mg $+$ ^{25}Mg $+$ ^{26}Mg. In Figure 6 we show the surface abundance evolution of the Mg isotopes for three different initial compositions, that use the new recommended rates for the ^{22}Ne+α reactions. In Table 5 we also present the Mg isotope ratios (in terms of ^{24}Mg:^{25}Mg:^{26}Mg) at the beginning and at the end of the TP-AGB phase for each model. Figure 6 and Table 5 show the influence of metallicity on the evolution of the Mg isotopes, where the effects of HBB become more significant at lower Z.

From Figure 5 we see the important result that using the new recommended rates for the ^{22}Ne+α reactions does not result in large changes to the production of ^{25}Mg and ^{26}Mg compared to the calculations performed using older estimates. For the solar metallicity model, the final surface Mg isotopic ratios are 70.8:13.5: 15.6 when using NACRE compared to 72.2:12.4:15.4 when using the new recommended rates. The only observable change is less ^{25}Mg but about the same amount (or just slightly less) ^{26}Mg. These results are consistently observed in the metal-poor AGB models, although the trends are stronger at lower metallicity.

To explain the above trends, we need to examine the behavior of the new rates compared to the NACRE and K94 rates. We produce less ^{25}Mg because the older estimates for the ^{22}Ne(α, n)^{25}Mg reaction are up to 40% faster at typical He-shell burning temperatures, i.e., $(250-400) \times 10^6$ K. Why the production of ^{26}Mg is reduced or remains about the same is not immediately obvious given that the new recommended rate is faster than both the NACRE (by up to 26%) and K94 (by 70%–100%) rates. The reason is again related to the (α, n) reaction, which releases neutrons during a TP, some of which are captured to produce ^{26}Mg, a process that is most efficient in the lowest Z models. In the solar metallicity models the production of ^{26}Mg is less dependent on the neutron flux, and we produce about the same when using the new recommended rate for the ^{22}Ne(α, γ)^{26}Mg reaction.

4.3. Stellar Yields

In the first row of Table 6 we present the stellar yields of ^{25}Mg and ^{26}Mg (in solar masses) for the 5 $M_\odot$ models of different Z, computed using the new recommended rates. In other rows we present the percentage difference between yields calculated with a different set of rates (as noted in the table), and our reference yields given in the first row.[9] In Figure 7 we show the percentage dif-

[9] According to [yield(i) − yield(ref)]/yield(ref) multiplied by 100, where i is one of the combinations of reaction rates described in § 2.
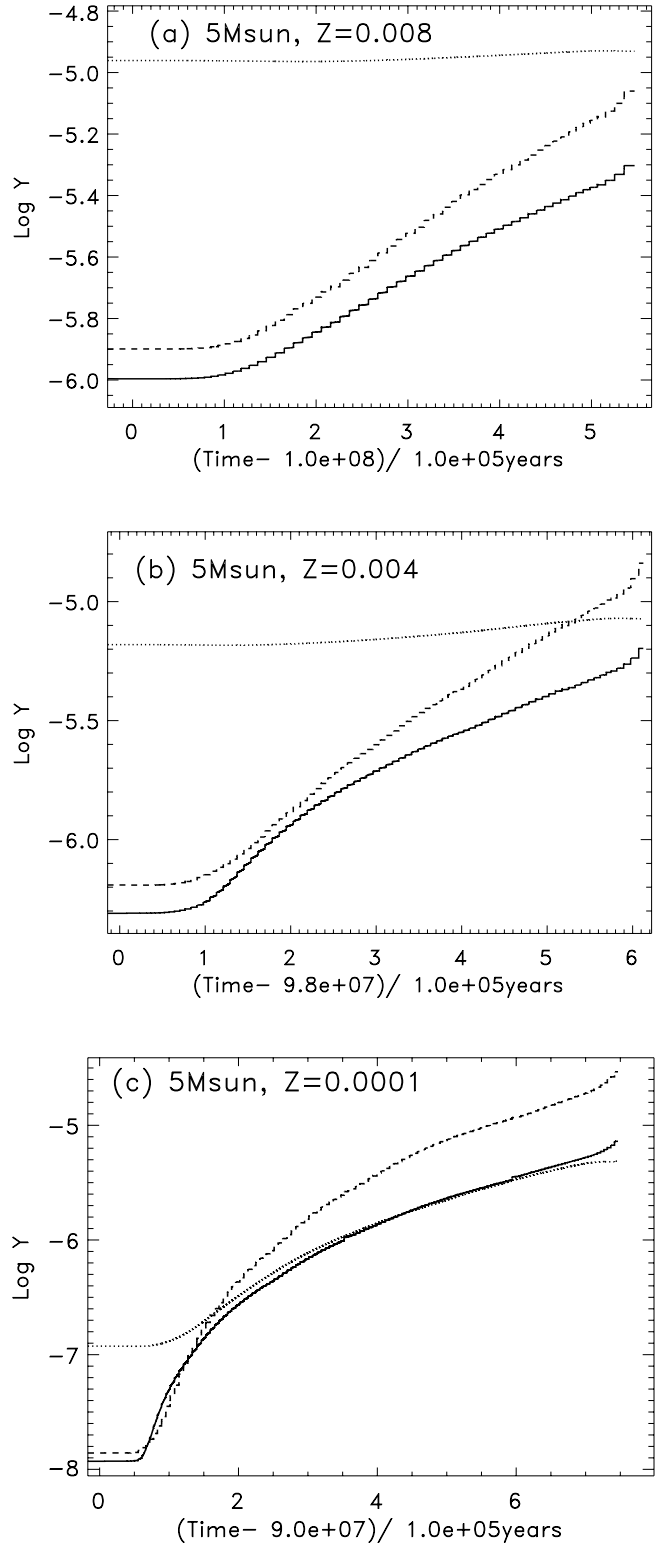

FIG. 6.—Surface abundance (in log mole fraction) of the Mg (^{24}Mg, *dotted lines*, ^{25}Mg and ^{26}Mg as in Fig. 5) isotopes as a function of time during the TP-AGB for models of different metallicity, using the new recommended rates.

ference between the stellar yields calculated using the new recommended rates (the reference), the new upper and lower limits and the NACRE recommended rates, for two different metallicities. The x-axis is atomic mass, and we present percentage differences for ^{22}Ne through to ^{31}P, with ^{26}Al included at 26.5. According to the definition of the percentage difference given

TABLE 6

TABLE 6

STELLAR YIELDS OF ^{25}Mg AND ^{26}Mg

^{22}Ne(α, γ)^{26}Mg	^{22}Ne(α, n)^{25}Mg	(5, 0.0001)	(5, 0.004)	(5, 0.008)	(5, 0.02)
Recommended............	Recommended	5.80($-$4)	4.84($-$4)	3.49($-$4)	6.49($-$5)
		2.28($-$3)*	1.11($-$3)*	6.84($-$4)*	1.17($-$4)*
Standard[a]	Standard[a]	$-$3.42	29.6	36.6	45.6
		9.05*	7.50*	3.51*	$-$5.95*
K94[b]	K94[b]	22.5	31.5	38.2	52.6
		9.80*	8.64*	5.68*	$-$2.99*
NACRE[c].....................	NACRE[c]	20.4	27.9	34.6	44.8
		15.3*	16.0*	15.9*	8.82*
Upper limit................	Upper limit	3.34	8.94	11.5	24.7
		13.8*	17.0*	18.9*	26.7*
Lower limit	Lower limit	$-$8.93	$-$7.95	$-$9.98	$-$14.7
		$-$14.2*	$-$16.2*	$-$17.5*	$-$16.6*
Lower limit	Upper limit	5.10	11.5	13.5	20.7
		0.46*	0.21*	$-$1.46*	$-$4.13*
Upper limit................	Lower limit	$-$9.95	$-$8.94	$-$11.2	$-$16.5
		2.47*	3.82*	4.96*	7.82*

NOTES.—In the first row we show the yields of ^{25}Mg (in roman font) and ^{26}Mg (indicated by asterisks) in solar masses for different stellar models ($M\ M_\odot$, Z) that use the new recommended rates for the ^{22}Ne+α reactions. In other rows we show the percentage difference between models computed using other estimates of the ^{22}Ne+α reactions and the yields from row 1 (see definition in the text).

[a] Standard case: Käppeler et al. (1994, K94) for the ^{22}Ne+α reactions; reaction rates for the NeNa and MgAl chains described in the Appendix.

[b] K94: For the ^{22}Ne+α reactions; NACRE recommended rates for the NeNa and MgAl chains.

[c] NACRE: Recommended rates for the ^{22}Ne+α reactions and the NeNa and MgAl chains.
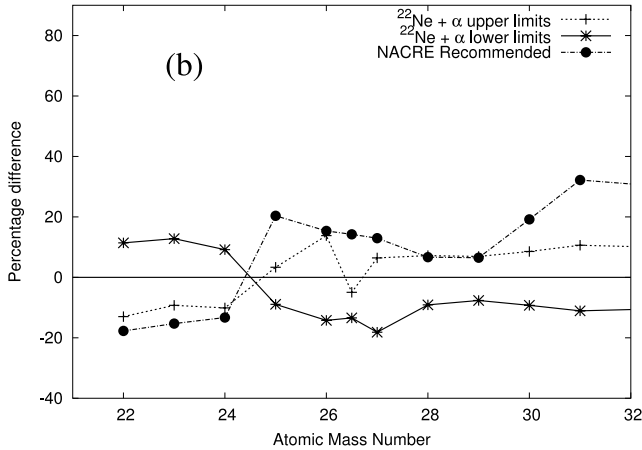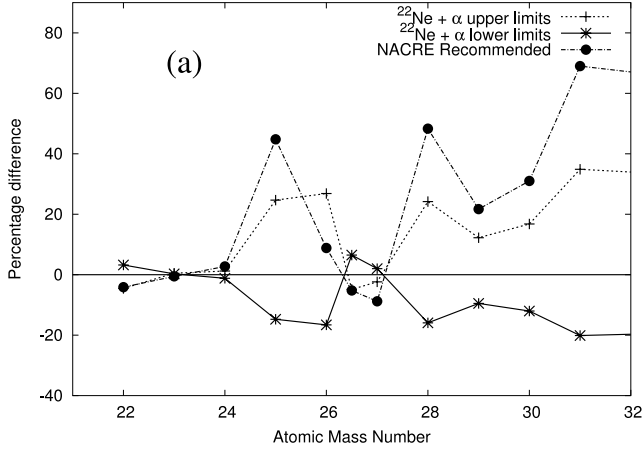

FIG. 7.—Percentage difference between stellar yields computed with the new recommended rates (the reference) and the new upper and lower limits and the NACRE recommended rates for the ^{22}Ne+α reactions. We show results for the (a) 5 $M_\odot$, $Z = 0.02$ and for (b) $Z = 0.0001$ model.
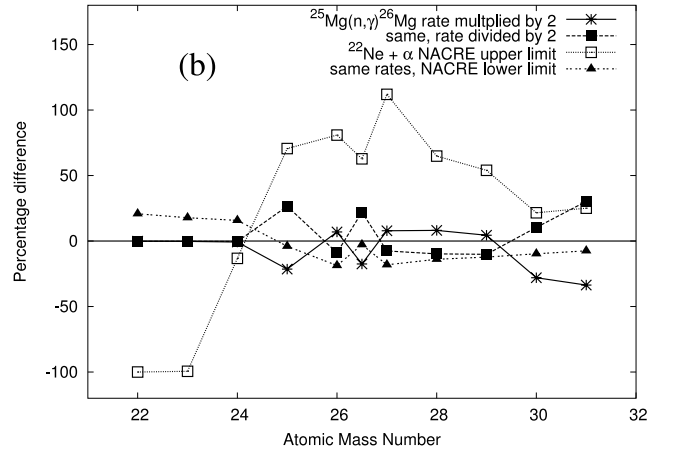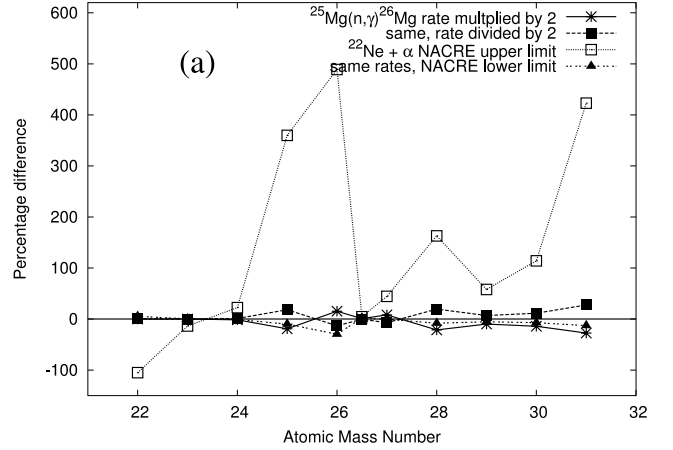

FIG. 8.—Same as Fig. 7, but now the reference yields were computed with the NACRE ^{22}Ne+α recommended rates, and we show percentage differences for models using the NACRE upper and lower limits. We also show results where the ^{25}Mg(n, γ)^{26}Mg reaction rate was varied by a factor of 2 each way.
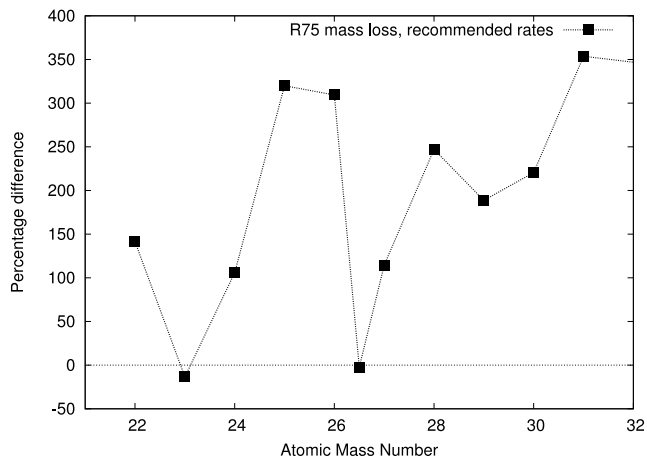
Fig. 9.—Percentage difference between the yields from the 5 $M_\odot$, $Z = 0.02$ model with R75 mass loss.

above, a positive difference means that that model produced (or destroyed) more of a given species compared to our reference case. To compare to the magnitude of the uncertainties associated the NACRE rates, in Figure 8 we show the percentage difference for models that use the NACRE recommended (the reference) and the NACRE upper and lower limits. We also vary the ^{25}Mg$(n, \gamma)^{26}$Mg reaction rate by a factor of 2 each way (see Fig. 8).

These figures show that using the new rates for the ^{22}Ne+α reactions results in considerably smaller uncertainties in the production of all isotopes between ^{22}Ne and ^{31}P compared to models that use the NACRE rates. For the ^{25}Mg and ^{26}Mg isotopes, differences of order ~400% in the case of the 5 $M_\odot$, $Z = 0.02$ model with the NACRE upper limits are reduced to less than 30%, when using the new upper limits. For models of lower metallicity, the uncertainties are even smaller (at most ~20%). Varying the ^{25}Mg$(n, \gamma)^{26}$Mg reaction rate given by Weigmann et al. (1976) by a factor of 2 each way results in differences of at most 33% in the production of ^{31}P, about 26% in the production of ^{25}Mg and about 15% in the production of ^{26}Mg for all models, regardless of metallicity. Note that the abundance of heavier isotopes are affected by neutron captures; hence the dependence on these reaction rates.

The percentage differences reported in Table 6 and shown in Figures 7 and 8 illustrate that the computed errors decrease with a decrease in the metallicity of the model. The reason could be that the yields significantly increase with an decrease in Z and hence changes to a larger number result in smaller differences than changes to a smaller number (in the case of the $Z = 0.02$ models). Also, the low-Z models have more TPs, and more efficient HBB means that the proton capture MgAl chain reactions have a greater overall effect on the stellar yields.

4.4. The Effect of Partial Mixing Zones and Varying the Mass-Loss Rate

The inclusion of a partial mixing zone (PMZ) at the deepest penetration of the TDU will mix protons from the envelope into the He intershell, producing a ^{13}C pocket. In the PMZ neutrons are liberated during the interpulse period by the neutron source reaction ^{13}C$(\alpha, n)^{16}$O, and the Mg isotopic abundances can be modified because of the activation of the chain of neutron captures starting from the abundant ^{22}Ne and proceeding through ^{23}Na to ^{24}Mg, ^{25}Mg, and ^{26}Mg. Given the high value of the neutron capture cross section of ^{25}Mg, with respect to those of ^{24}Mg and ^{26}Mg

(see Bao et al. 2000), neutron captures in the ^{13}C pocket produce ^{24}Mg and ^{26}Mg, while depleting ^{25}Mg. The details of how the ^{13}C pocket forms is still unknown, although various mechanisms have been proposed; see Lugaro et al. (2004) for a wider discussion. In nucleosynthesis studies, the extent of the pocket is usually set as a free parameter with typical values ~1/15 the mass of the He intershell (Gallino et al. 1998; Goriely & Mowlavi 2000). In intermediate-mass stars, the mass of the He intershell is smaller by about an order of magnitude compared to lower mass stars, and hence the importance of the ^{13}C pocket may be lessened (Gallino et al. 1998). As done in previous nucleosynthesis studies (Gallino et al. 1998; Goriely & Mowlavi 2000; Lugaro et al. 2004), we artificially include in the postprocessing calculation a PMZ of constant mass $M_{pmz} = 1 \times 10^{-4}$ $M_\odot$ in the 5 $M_\odot$, $Z = 0.02$ model. We chose a proton profile in which the number of protons decreases exponentially with the mass depth below the base of the convective envelope exactly in the same way as described in Lugaro et al. (2004). The mass of the He intershell decreases with evolution, and for the solar metallicity model, the final He-shell mass is about 0.001, so that our PMZ region is at maximum 1/10th of the He intershell.

The inclusion of the PMZ produces small percentage differences (less than ~10%) for most species, with the exception of ^{31}P (28%) and the particle g (104%). Hence, there are no changes to the ^{25}Mg and ^{26}Mg yields with the introduction of a PMZ of $M_{pmz} = 1 \times 10^{-4}$ $M_\odot$. This conclusion is consistent with the results obtained by Lugaro et al. (1999) for the elements Si and Ti and can be extended to all intermediate-mass elements. There are two reasons for this. First, since elements lighter than iron have very small neutron capture cross sections, as much as 3 orders of magnitude smaller as compared to those of nuclei heavier than iron, their abundances are not strongly affected by the neutron flux in the ^{13}C pocket. In fact, the changes in the abundances of intermediate-mass elements in the ^{13}C pocket are at maximum of 1 order of magnitude, while the abundances of heavy elements are produced by up to 3 orders of magnitude of their initial values (see, e.g., Table 2 of Lugaro et al. [1999]). Second, the ^{13}C pocket is engulfed and diluted (of factors between 1/20 and 1/10) by the next growing convective pulse, and is thus mixed with material already α-processed during the previous pulses, and with the ashes of the H-burning shell. During this dilution process the signature on intermediate-mass elements of neutron captures in the ^{13}C pocket is completely lost. As for proton captures occurring in the PMZ region just after the mixing of protons has occurred, they are expected to destroy ^{25}Mg only in the upper layer of the PMZ where the number of protons is higher than 0.5 (see Fig. 1 of Goriely & Mowlavi [2000]). Thus they do not produce a strong effect when this region is diluted in the He intershell, unless the proton profile is very different from the one assumed here.

We also experiment with varying the mass-loss rate. The results for the $Z = 0.02$ case with R75 mass loss are shown in Figure 9. In this figure we observe large differences of a few hundred percent for most species. For the 5 $M_\odot$, $Z = 0.0001$ R75 model we use two different choices of the ^{22}Ne+α reaction rates, as described in Figure 10. The R75 model has fewer TPs than the VW93 case, which results in smaller yields: hence the negative values. We see from Figure 10 that changing the reaction rates has only a small effect on the yields, compared to the change induced by varying the mass-loss rate. This was also well demonstrated by Ventura & D'Antona (2005b) for intermediate-mass AGB stars of $Z = 0.001$. The species most affected by the change in mass-loss law are ^{23}Na, ^{24}Mg, and ^{26}Al, because the abundances of these isotopes depend on the duration of the HBB phase.
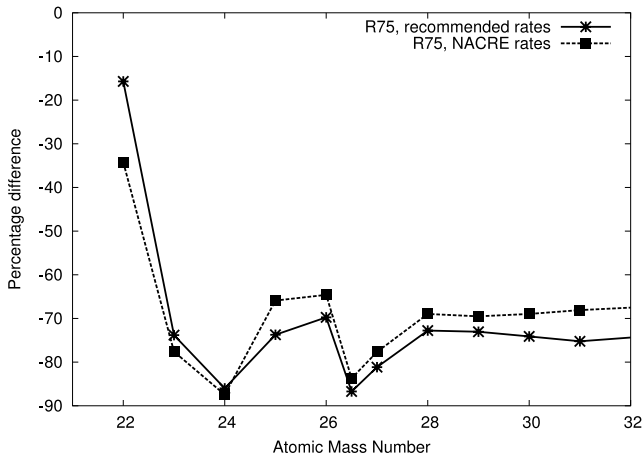
FIG. 10.—Percentage difference between the yields from the 5 $M_\odot$, $Z = 0.0001$ model with VW93 mass loss and two models with R75 mass loss.

4.5. *Other Model Uncertainties*

With regard to the reaction rates, uncertainties remain related to the proton capture rates for the NeNa and MgAl chains that modify the abundances of these nuclei because of HBB. Table 6 shows that updating these proton capture rates from our standard set to those recommended by NACRE did not produce any major modifications on the Mg isotopes, since variations are only a few percent. The variations are small because the reaction rates in the MgAl chain that affect the Mg isotopic ratios the most are similar between NACRE and our standard choices, with differences typically less than 40%. A detailed study of the impact of the uncertainties of proton capture reactions on the results produced by HBB on the Ne, Na, Mg, and Al isotopes is underway (R. G. Izzard et al. 2006, in preparation).

We discussed in § 1 that major uncertainties are still present in the computation of the stellar models, in particular in relation to the treatment of convection and of convective boundaries. When our results for the 5 $M_\odot$, $Z = 0.004$ model, which are calculated using MLT with $\alpha = 1.75$, are compared with those produced by a 5 $M_\odot$, $Z = 0.001$ model computed using the full spectrum of turbulence (FST) prescription for convective regions by Ventura & D'Antona (2005a), we find that the final abundances of the Mg isotopes are lower in the FST case with respect to our case by about 2 dex for ^{24}Mg, 1 dex for ^{25}Mg, and 0.4 dex for ^{26}Mg (including the contribution of radioactive ^{26}Al). In particular, in our case, ^{25}Mg and ^{26}Mg are produced in similar abundances by the effect of the ^{22}Ne+α reactions and deep TDU, while, in the FST case, the production of nuclei of mass $A = 26$ (^{26}Al and ^{26}Mg) is favored with respect to that of ^{25}Mg by the combined effect of strong HBB and weak TDU (P. Ventura 2005, private communication). These different behaviors should be tested against data from presolar grains and, using GCE models, against the observations of the Mg isotopes in stars, and also the galactic abundance of the radioactive nucleus ^{26}Al, as obtained by the galactic gamma line at 1.809 MeV (Diehl et al. 2004).

Herwig (2004b) implements a diffusive convective overshoot scheme at all convective borders in his AGB models (see also Herwig et al. 1997), which results in a considerably different stellar structure to our models of the same mass and metallicity. The most significant differences are hotter TPs and deeper TDU (where $\lambda \gtrsim 1$), as well as the mixing of some CO core material into the flash-driven convective pocket. If we compare the surface ^{25}Mg and ^{26}Mg mass fractions after the 14th TP, we find that these isotopes are enriched by up to 5 times more in Herwig's 5 $M_\odot$,

$Z = 0.0001$ model compared to our equivalent case with the new recommended rates. These differences are much larger than those introduced by the ^{22}Ne+α-capture rates. Herwig also reports $X(^{26}$Mg$)/X(^{25}$Mg$) > 1$ after 14 TPs, whereas after the same number of pulses we find this ratio to be less than unity. This is because hotter TPs result in a stronger activation of the ^{22}Ne$(\alpha, n)^{25}$Mg reaction; hence, more neutrons are released that are captured by ^{25}Mg to form ^{26}Mg.

5. DISCUSSION AND CONCLUSIONS

The main important result of the present study is that the reduction of the uncertainties on the ^{22}Ne+α-reaction rates has allowed us to considerably reduce the uncertainties coming from these rates on the production of isotopes from Mg to P in AGB stars of intermediate mass. The uncertainties on the Mg yields are now at a level of ∼30%, much lower than those obtained when using the NACRE upper or lower limits. The yields of ^{25}Mg and ^{26}Mg are 20%–45% and 9%–16%, respectively, smaller with the new rates, as compared to NACRE. The uncertainties have also been reduced for species heavier than Mg, where, for example, the uncertainty on the production of P in solar metallicity models is now at a level of 35%, much lower than the 400% obtained when using the NACRE upper limit. These results are clearly illustrated by Figures 7 and 8 and in Table 6.

From our analysis it would appear that among the uncertainties related to the stellar models, those coming from the treatment of convection and of the mass loss are the largest. We described earlier that these are enormous when compared to the current uncertainties coming from the ^{22}Ne+α-reaction rates. Much effort is needed to improve the situation for AGB models, in particular with respect to convection, by trying to evaluate and reduce the uncertainties, perhaps by exploiting all the available observational constraints.

Our new evaluation of the ^{22}Ne+α-reaction rates will encourage much future work, as these rates are important for many nucleosynthetic processes and sites. The ^{22}Ne$(\alpha, n)^{25}$Mg reaction is an important source of neutrons both during the final evolutionary stages of massive stars and during the AGB phase of low- to intermediate-mass stars. It is responsible for the production of heavy *s*-process elements in these environments (Gallino et al. 1998; Rauscher et al. 2002). The new rate and its uncertainties have to be tested in relation to this process. Moreover, the smaller uncertainties of the rates presented here with respect to those in NACRE appear to rule out the possibility that the production of the relatively abundant *p*-only isotopes of Mo and Ru could be related to a high value of the ^{22}Ne$(\alpha, n)^{25}$Mg rates (Costa et al. 2000).

It is important to study the relative production of ^{25}Mg and ^{26}Mg, as we have done in Table 6, because both spectroscopic observations and the analysis of presolar grains are able to separate these two isotopes. Also the contribution of radioactive ^{26}Al to the abundance of ^{26}Mg has to be carefully evaluated. In particular, one presolar spinel grain (OC2; Zinner et al. 2005) appears to bear the signature of nucleosynthesis in intermediate-mass AGB stars, with excesses in both ^{25}Mg and ^{26}Mg. A future application of our present work will be to compare our detailed results to the composition of this grain, extending the study to the oxygen isotopic ratios in AGB stars and their uncertainties, as these are also measured in the grain.

APPENDIX

DETAILS OF THE REACTION RATES USED IN THE REFERENCE CASE

Most of the 506 reaction rates come from the REACLIB Data Tables (ver. 1991). The updates made to the proton, α, and neutron capture rates are detailed in Lugaro et al. (2004) with one exception. We have since updated the $^{14}N(\alpha, \gamma)^{18}F$ reaction rate to that given by Görres et al. (2000). This reaction rate set is considered our *standard* set. Note that in our standard reaction rate set, we use the $^{22}Ne+\alpha$ rates given by Käppeler et al. (1994) and Drotleff et al. (1993).

We have also used NACRE rates for many of the reactions involved in the NeNa and MgAl chains. In Table 7 we list the reactions that we changed to those given by NACRE; we also include the reference for that rate used in the standard reaction rate set for comparison. CF88 refers to Caughlan & Fowler (1988).

TABLE 7
PROTON CAPTURE RATES CHANGED TO THOSE GIVEN BY NACRE

Reaction	Reference
$^{19}F(p, \gamma)^{20}Ne$...	1
$^{20}Ne(p, \gamma)^{21}Ne$	1
$^{21}Ne(p, \gamma)^{22}Na$	2
$^{22}Ne(p, \gamma)^{23}Na$ [a,b]	2
$^{23}Na(p, \gamma)^{24}Mg$	2
$^{23}Na(p, \alpha)^{20}Ne$	2
$^{24}Mg(p, \gamma)^{25}Al$	3
$^{25}Mg(p, \gamma)^{26}Al^{g/i}$	4, 5
$^{26}Mg(p, \gamma)^{27}Al$	5
$^{26}Al^{g}(p, \gamma)^{27}Si$	6, 7
$^{26}Al^{i}(p, \gamma)^{27}Si$	1
$^{27}Al(p, \gamma)^{28}Si$	5, 8
$^{27}Al(p, \alpha)^{24}Mg$	6, 8

[a] But beware the error in the NACRE analytical fit for $0.15 \geq T_9 \geq 2.0$ compared to the tabulated rate.
[b] The rate given by El Eid & Champagne (1995) contains a typographical error for the first term.
REFERENCES.—(1) CF88; (2) El Eid & Champagne 1995; (3) Powell et al. 1999; (4) Iliadis et al. 1996; (5) Iliadis et al. 1990; (6) Champagne et al. 1993; (7) Vogelaar et al. 1996; (8) Timmermann et al. 1988.

REFERENCES

Anders, E., & Grevesse, N. 1989, Geochim. Cosmochim. Acta, 53, 197
Angulo, C., et al. 1999, Nucl. Phys. A, 656, 3
Ashenfelter, T., Mathews, G. J., & Olive, K. A. 2004, Phys. Rev. Lett., 92, 041102
Bao, Z. Y., Beer, H., Käppeler, F., Voss, F., Wisshak, K., & Rauscher, T. 2000, At. Data Nucl. Data Tables, 76, 70
Berman, B. L., van Hemert, R. L., & Bowman, C. D. 1969, Phys. Rev. Lett., 23, 386
Busso, M., Gallino, R., & Wasserburg, G. J. 1999, ARA&A, 37, 239
Campbell, S. W., Fenner, Y., Karakas, A. I., Lattanzio, J. C., & Gibson, B. K. 2005, Nucl. Phys. A, 758, 272
Cannon, R. C. 1993, MNRAS, 263, 817
Caughlan, G. R., & Fowler, W. A. 1988, At. Data Nucl. Data Tables, 40, 283 (CF88)
Champagne, A. E., Brown, B. A., & Sherr, R. 1993, Nucl. Phys. A, 556, 123
Chieffi, A., & Limongi, M. 2002, ApJ, 577, 281
———. 2004, ApJ, 608, 405
Costa, V., Rayet, M., Zappalá, R. A., & Arnould, M. 2000, A&A, 358, L67
Dababneh, S., et al. 2003, Phys. Rev. C, 68, 025801
Diehl, R., Cerviño, M., Hartmann, D. H., & Kretschmer, K. 2004, NewA Rev., 48, 81
Drotleff, H. W., et al. 1993, ApJ, 414, 735
El Eid, M. F., & Champagne, A. E. 1995, ApJ, 451, 298

Fenner, Y., Campbell, S., Karakas, A. I., Lattanzio, J. C., & Gibson, B. K. 2004, MNRAS, 353, 789
Fenner, Y., Gibson, B. K., Lee, H.-C., Karakas, A. I., Lattanzio, J. C., Chieffi, A., Limongi, M., & Yong, D. 2003, Publ. Astron. Soc. Australia, 20, 340
Fenner, Y., Murphy, M. T., & Gibson, B. K. 2005, MNRAS, 358, 468
Frost, C. A., Cannon, R. C., Lattanzio, J. C., Wood, P. R., & Forestini, M. 1998, A&A, 332, L17
Frost, C. A., & Lattanzio, J. C. 1996, ApJ, 473, 383
Gallino, R., Arlandini, C., Busso, M., Lugaro, M., Travaglio, C., Straniero, O., Chieffi, A., & Limongi, M. 1998, ApJ, 497, 388
Gay, P. L., & Lambert, D. L. 2000, ApJ, 533, 260
Giesen, U., et al. 1994, Nucl. Phys. A, 567, 146
Goriely, S., & Mowlavi, N. 2000, A&A, 362, 599
Görres, J., et al. 2000, Phys. Rev. C, 62, 055801
Harms, V., Kratz, K.-L., & Wiescher, M. 1991, Phys. Rev. C, 43, 2849
Herwig, F. 2004a, ApJ, 605, 425
———. 2004b, ApJS, 155, 651
———. 2005, ARA&A, 43, 435
Herwig, F., Blöcker, T., Schönberner, D., & El Eid, M. 1997, A&A, 324, L81
Iliadis, C., Buchmann, L., Endt, P. M., Herndl, H., & Wiescher, M. 1996, Phys. Rev. C, 53, 457
Iliadis, C., et al. 1990, Nucl. Phys. A, 512, 509

Jaeger, M., Kunz, R., Mayer, A., Hammer, J. W., Staudt, G., Kratz, K. L., & Pfeiffer, B. 2001, Phys. Rev. Lett., 87, 202501

Johnson, J. A., Herwig, F., Beers, T. C., & Christlieb, N. 2005, Nucl. Phys. A, 758, 221

Käppeler, F., et al. 1994, ApJ, 437, 396 (K94)

Karakas, A. I., & Lattanzio, J. C. 2003, Publ. Astron. Soc. Australia, 20, 279

Karakas, A. I., Lattanzio, J. C., & Pols, O. R. 2002, Publ. Astron. Soc. Australia, 19, 515

Koehler, P. 2002, Phys. Rev. C, 66, 055805

Lattanzio, J. C. 1986, ApJ, 311, 708

Lattanzio, J. C., Frost, C. A., Cannon, R., & Wood, P. R. 1996, Mem. Soc. Astron. Italiana, 67, 729

Lodders, K. 2003, ApJ, 591, 1220

Lugaro, M., Ugalde, C., Karakas, A. I., Görres, J., Wiescher, M., Lattanzio, J. C., & Cannon, R. C. 2004, ApJ, 615, 934

Lugaro, M., Zinner, E., Gallino, R., & Amari, S. 1999, ApJ, 527, 369

Mowlavi, N. 1999, A&A, 344, 617

Murphy, M. T., Webb, J. K., Flambaum, V. V., Dzuba, V. A., Churchill, C. W., Prochaska, J. X., Barrow, J. D., & Wolfe, A. M. 2001, MNRAS, 327, 1208

Powell, D. C., Iliadis, C., Champagne, A. E., Grossmann, C. A., Hale, S. E., Hansper, V. Y., & McLean, L. K. 1999, Nucl. Phys. A, 660, 349

Rauscher, T., Heger, A., Hoffman, R. D., & Woosley, S. E. 2002, ApJ, 576, 323

Reddy, B. E., Tomkin, J., Lambert, D. L., & Allende Prieto, C. 2003, MNRAS, 340, 304

Reimers, D. 1975, in Problems in Stellar Atmospheres and Envelopes, ed. B. Baschek, W. H. Kegel, & G. Traving (New York: Springer), 229

Sackmann, J.-I., & Boothroyd, A. I. 1992, ApJ, 392, L71

Stancliffe, R., Tout, C. A., & Pols, O. R. 2004, MNRAS, 352, 984

Thielemann, F.-K., Arnould, M., & Truran, J. W. 1986, in Advances in Nuclear Astrophysics, ed. E. Vangioni-Flam et al. (Gif-sur-Yvette: Editions Fron-tières), 525

Timmermann, R., Becker, H. W., Rolfs, C., Schröder, U., & Trautvetter, H. P. 1988, Nucl. Phys. A, 477, 105

Timmes, F. X., Woosley, S. E., & Weaver, T. 1995, ApJS, 98, 617

Vassiliadis, E., & Wood, P. R. 1993, ApJ, 413, 641 (VW93)

Ventura, P., & D'Antona, F. 2005a, A&A, 431, 279

———. 2005b, A&A, 439, 1075

Vogelaar, R. B., et al. 1996, Phys. Rev. C, 53, 1945

Weigmann, H., et al. 1976, Phys. Rev. C, 14, 1328

Wolke, K., et al. 1989, Z. Phys. A., 334, 491

Woosley, S. E., & Weaver, T. A. 1995, ApJS, 101, 181

Yong, D., Aoki, W., & Lambert, D. L. 2006, ApJ, 638, 1018

Yong, D., Grundahl, F., Lambert, D. L., Nissen, P. E., & Shetrone, M. D. 2003a, A&A, 402, 985

Yong, D., Lambert, D. L., & Ivans, I. 2003b, ApJ, 599, 1357

Zinner, E., Nittler, L. R., Hoppe, P., Gallino, R., Straniero, O., & Alexander, C. M. O'D. 2005, Geochim. Cosmochim. Acta, 69, 4149